Thermochimica Acta, 51 (1981) 199—224
Elsevier Scientific Publishing Company, Amsterdam — Printed in The Netherlands

SEM OBSERVATION OF THE THERMAL DECOMPOSITION PROCESSES OF $KClO_4$, $KClO_3$, $KBrO_3$, KIO_4 AND KIO_3 IN THE PRESENCE OF α-Fe_2O_3 AND α-Al_2O_3

RYUSABURO FURUICHI, TADAO ISHII, ZENZO YAMANAKA and MASAHIDE SHIMOKAWABE

Department of Applied Chemistry, Faculty of Engineering, Hokkaido University, 060 Sapporo (Japan)

(Received 27 May 1981)

ABSTRACT

The effect of the addition of α-Fe_2O_3 and α-Al_2O_3 on the thermal decomposition of five salts of halogen oxoacids ($KClO_4$, $KClO_3$, $KBrO_3$, KIO_4 and KIO_3) was studied by DTA of salt—oxide mixtures and by SEM observation and X-ray analysis of partly reacted mixtures obtained during the course of the decomposition process. DTA results suggested that α-Fe_2O_3 gives rise to solid state decomposition of the salts before they melt, except in the decomposition of KIO_4 into KIO_3, in contrast with the liquid state decomposition after melting in the pure salt systems. In order to identify the occurrence of solid state decomposition in α-Fe_2O_3—salt systems, SEM observations were performed for samples obtained after decomposition to various extents by heating up to various temperatures on the DTA curves. From comparison of SEM photographs of α-Fe_2O_3—salt systems with those of pure salts and α-Al_2O_3—salt systems, it was found that α-Fe_2O_3 shows observable indications of the solid state decomposition of the salts at the initial stage.

INTRODUCTION

In previous papers [1—3], the authors have reported the results of DTA experiments on the effect of the addition of oxides, such as α-Fe_2O_3, α-Al_2O_3, CuO and NiO, on the thermal decomposition of salts of halogen oxoacids, oxalates, azide, permanganate, and oxides. It has been found that α-Fe_2O_3 shows a remarkable catalytic acceleration effect giving a large decrease in the thermal decomposition temperature of $KClO_4$, $KClO_3$, $KBrO_3$ and KIO_4. In the cases without α-Fe_2O_3, these oxoacids, with the exception of KIO_4, showed the endothermic DTA peak due to melting and then the sharp exothermic peak due to decomposition in the liquid phase. The addition of α-Fe_2O_3, however, resulted in a decrease in the exothermic peak temperature below the melting temperature of the salts. The DTA results mentioned above would lead to an assumption that the decomposition occurred in the solid state by the addition of α-Fe_2O_3. This is in agreement with the conclusion drawn by Rudloff and Freeman [4] for the catalytic decomposition of $KClO_4$ and $KClO_3$.

In the present study, SEM observation and X-ray analysis of samples obtained at various temperatures in the course of the thermal decomposition

0040-6031/81/0000—0000/$02.75

were carried out in order to understand the effect of the addition of α-Fe_2O_3 on the decomposition processes of $KClO_4$, $KClO_3$, $KBrO_3$, KIO_4 and KIO_3. Considerable differences in the decomposition behaviors were observed between pure salt and salt mechanically mixed with α-Fe_2O_3. Since the salts of these oxoacids were used in a powdery state, however, the kinetic data of the decomposition could not be obtained from SEM photographs as in the case of NH_4ClO_4 single crystal [5,6].

EXPERIMENTAL

Additives

α-Fe_2O_3. Ferric oxide was prepared from $FeC_2O_4 \cdot 2\,H_2O$ by calcining it in flowing air (100 ml min^{-1}) at 500°C for 1 h. The oxide formed was ground to pass through a 200 mesh sieve. The X-ray diffraction pattern of the oxide was identified as α-Fe_2O_3 with reference to ASTM 13-534.

α-Al_2O_3. α-Al_2O_3 was obtained from activated alumina (Merck) by heating it in static air at 1300°C for 3 h. The X-ray pattern coincided with ASTM 10-173. α-Al_2O_3 powders passed through 200 mesh sieve were employed as an additive and the reference material of DTA experiments.

NiO. Thermal decomposition of $NiCO_3 \cdot 2\,Ni(OH)_2 \cdot 4\,H_2O$ was carried out to prepare the oxide under the conditions of flowing O_2 (100 ml min^{-1}) at 500°C for 1 h. The oxide obtained was confirmed to be NiO by X-ray analysis (ASTM 4-835).

Figure 1 shows SEM photographs of α-Al_2O_3, α-Fe_2O_3 and NiO.

Salts of halogen oxoacids

Five salts ($KClO_4$, $KClO_3$, $KBrO_3$, KIO_4 and KIO_3) were employed for the experiments. All were commercial reagents from Kanto Chemical Co. and were used without further purification. The mixing ratio of salt to additive was 1 : 1 by weight. Mechanical mixing was carried out in an agate mortar for 30 min. Pure salt without additive was also pretreated in the mortar for 30 min to obtain the same grinding condition as the mixture.

DTA

Apparatus and procedures have been previously described in detail [7]. The apparatus consisted of two quartz tubes (i.d. = 10 mm) placed vertically in an electric tube furnace. The sample was packed in the quartz tube which could be quenched rapidly with cold water to stop the reaction. The experimental conditions were: weight of sample and reference material (α-Al_2O_3) = 1 g, heating rate = 4.6°C min^{-1}, chromel–alumel thermocouple 0.3 mm diam, and atmosphere = static air.

X-Ray diffraction

A Geigerflex type 2001 diffractometer (Rigaku Denki Co.) was used for the powder X-ray diffraction of the samples. Samples were obtained by

quenching them in the DTA quartz tube to room temperature from various temperatures during the course of the reaction. The diffraction conditions were: target = Co, voltage = 35 kV, current = 10mA, and scanning speed = 1° min^{-1}.

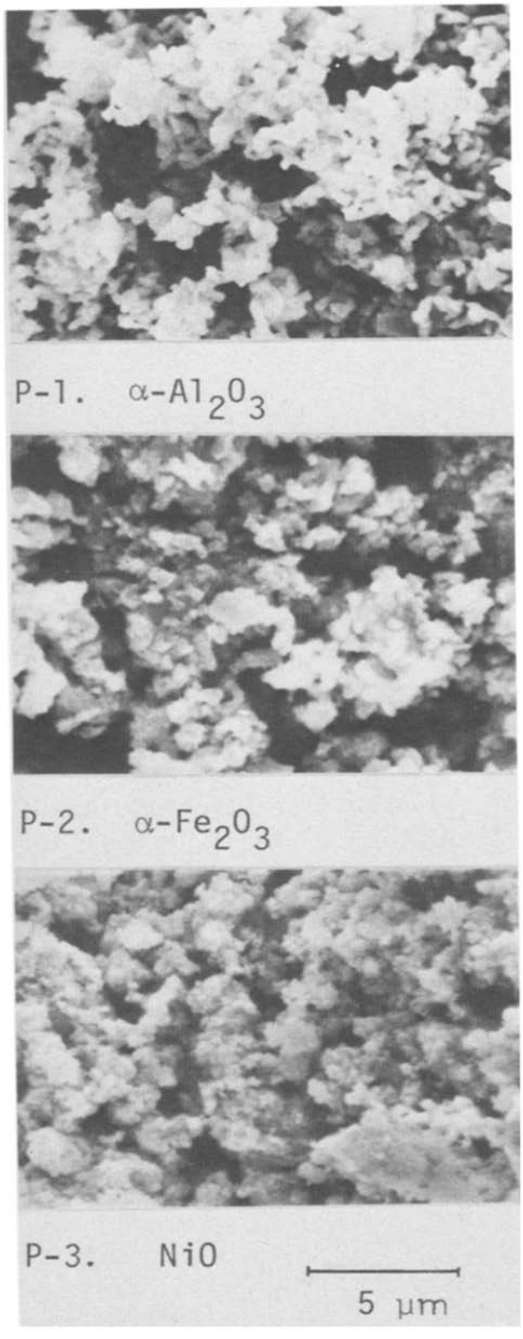

Fig. 1. SEM photographs of oxides used as the additive.

SEM

SEM photographs were taken by using a part of sample for X-ray diffraction. Sample powders were mounted on a cylindrical aluminum block with adhesive tape. The sample was spattered with thin Au film (15—20 nm) by the use of an Ion Coater type 1B-3 (Eiko Engineering Co.) operated at a spattering current of 6 mA. The SEM apparatus, Mini-SEM Model MSM-4 (Akashi Seisakusho Ltd.), was operated at 15 kV.

RESULTS AND DISCUSSION

Potassium perchlorate

Figure 2 shows the DTA curves of the $KClO_4$ systems. The numbered circles on the curves correspond to the temperatures at which samples for SEM and X-ray analysis are taken from DTA apparatus. Figures (2-A)—(2-D) show SEM photographs, which are appended with X-ray results and the temperature at which the sample was taken.

Pure $KClO_4$

Figure 2, curve (2-A) is the DTA curve of $KClO_4$ without additive. As reported previously [1,2], the endothermic peak at 310°C corresponds to crystallographic transformation, the sharp endothermic peak at 605°C is due to melting and the sharp exothermic peak at 620°C results from the liquid state decomposition of $KClO_4$. The thermal decomposition process of pure $KClO_4$ was followed by taking ten SEM photographs shown in Fig. (2-A). The first photograph (P-1) in the figure shows the perchlorate powders at room temperature before heating. It can be observed that there are small particles on the smooth surface of the large $KClO_4$ particle with cracks. P-2 shows the sample heated to 425°C after the reversible crystallographic transformation from the rhombic to the cubic form of $KClO_4$, corresponding to the endothermic DTA peak at 310°C. Since the pronounced differences cannot be seen between P-1 and P-2, the transformation is found to give no change in the surface and the form of the $KClO_4$ particle. P-3 was taken after heating to 495°C at which temperature the decomposition product, KCl, was not detected by X-ray analysis. P-3 shows that the small particles seen on P-1 and P-2 change shape from angular to round (mushroom-like) and adhere to the surface of large particles of $KClO_4$. This change may indicate that solid $KClO_4$ began to soften at temperatures before the appearance of the endothermic DTA peak (605°C) due to melting. P-4, taken for a sample heated to 510°C, shows a similar view to that of P-3, but the development of surface roughening is recognized on the $KClO_4$ as shown in P-4′ which is a 2 × magnification of P-4. P-5 and P-6 show samples heated to 570 and 580°C just before the start of the melting DTA peak. These photographs indicate the disappearance of the mushroom-like particles and the surface roughening observed in P-4, the formation of a smooth surface and the progress of softening of $KClO_4$. The black pentagonal area in P-6 is due to electron beam damage of the Au layer on the sample. P-7 shows the sample heated to

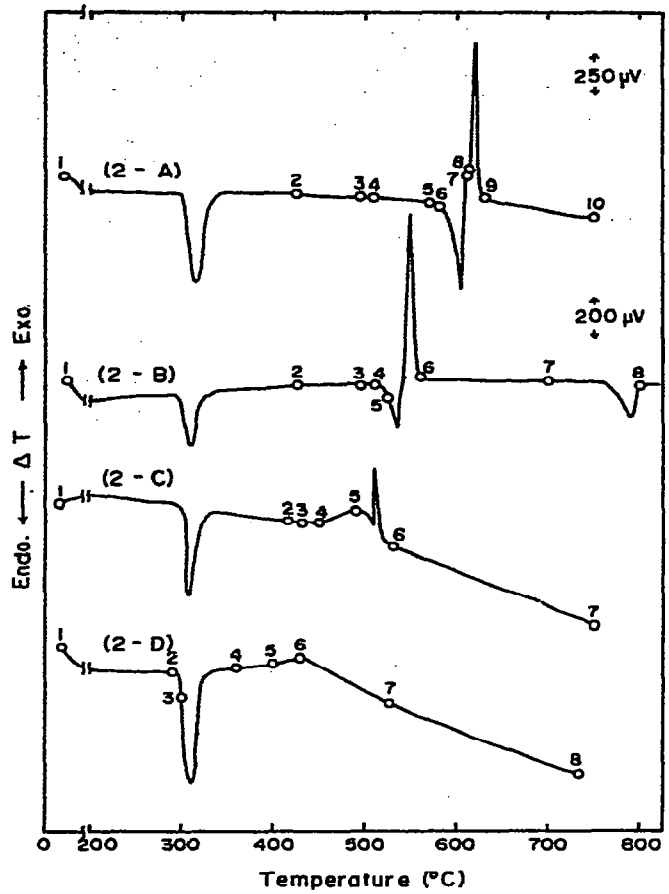

Fig. 2. DTA curves of $KClO_4$ systems. (2-A), $KClO_4$; (2-B), $KClO_4$ + α-Al_2O_3; (2-C), $KClO_4$ + α-Fe_2O_3; (2-D), $KClO_4$ + NiO. Heating rate, 4.6°C min^{-1} atmosphere, static air; mixing ratio, 1 : 1 by weight. Circles indicate the temperatures at which the samples were removed and the numbers appended to the circles correspond to photograph numbers in Figs. (2-A)—(2-D).

610°C just after the melting DTA peak at 605°C. The formation of a small amount of KCl was detected by X-ray analysis of this sample. The appearance of small particles is observed in P-7. P-8 shows the sample heated to 615°C. This sample gave an increased diffraction line intensity of KCl. It is found that small particles are produced with the progress of the decomposition. At 630°C, after the sharp exothermic DTA peak of decomposition, the sample transforms to pure KCl, which can be seen in P-9 as a large particle formed from sintering of the small particles seen in P-8. P-10 shows the formation of a large KCl crystal with smooth surface at 750°C.

(ii) $KClO_4$—α-Al_2O_3 mixture

Figure 2, curve (2-B) is the DTA curve and Fig. (2-B) shows SEM photographs of the decomposition process of the mixture. The pattern of the DTA curve is identical to that of $KClO_4$ alone; crystallographic transformation (endotherm at 310°C), melting (endotherm at 530°C), liquid phase decom-

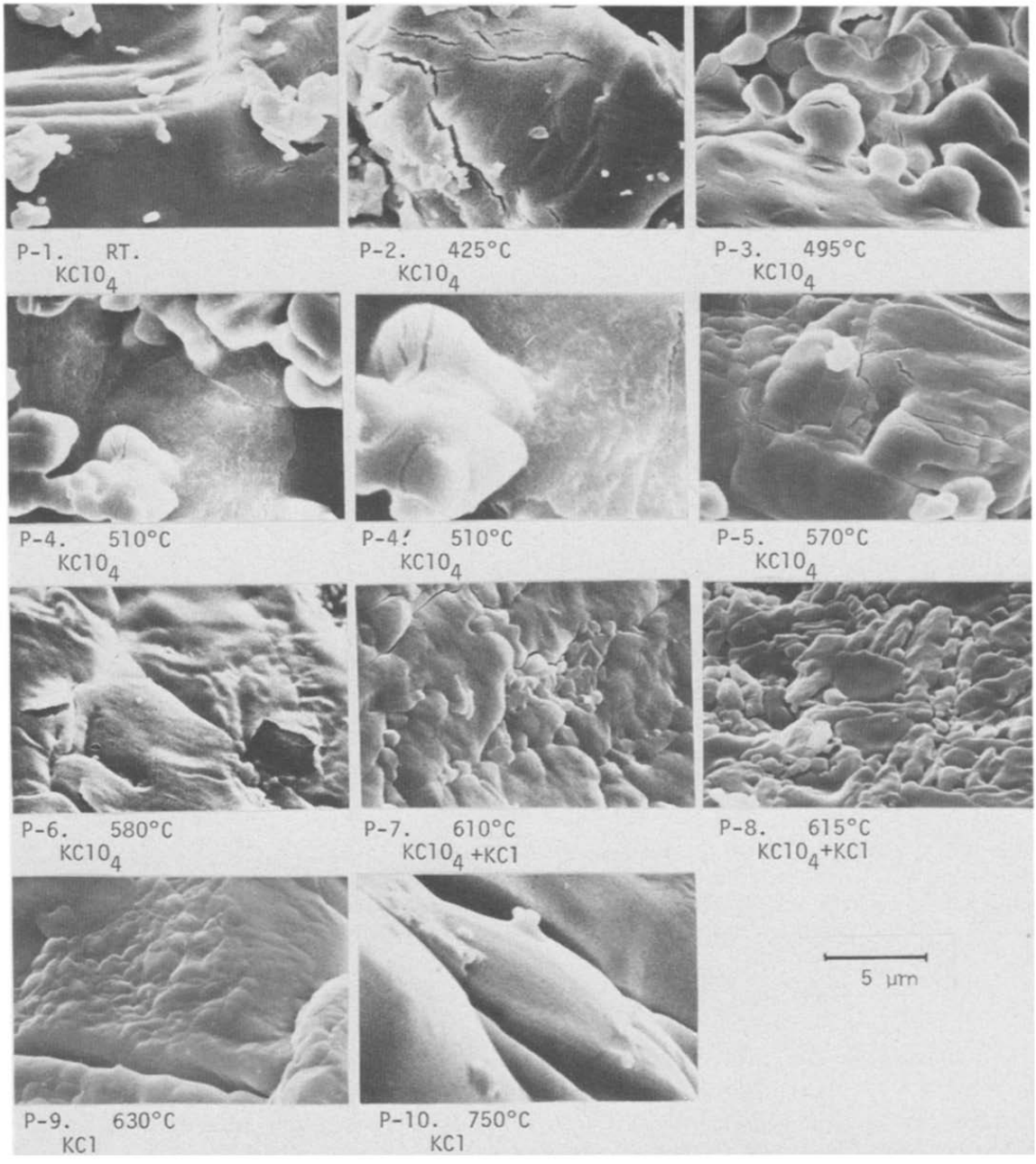

Fig. (2-A). SEM photographs showing the thermal decomposition of pure $KClO_4$. Heating temperature and X-ray result of the samples are indicated below each photograph. The length of bar corresponds to 10 μm for P-4'.

position (exotherm at 550°C), and fusion of KCl (endotherm at 790°C). The peak temperatures of melting and decomposition of the mixed system are found to be lower by about 70°C than those for pure $KClO_4$.

Figure (2-B), P-1 shows the mixture of $KClO_4$ and α-Al_2O_3 before decomposition. It is observed that the small white α-Al_2O_3 particles (refer to Fig. 1, P-1) are scattered on a large $KClO_4$ crystal. P-2 and P-3 indicate that samples heated up to 425 and 495°C above the crystallographic transformation tem-

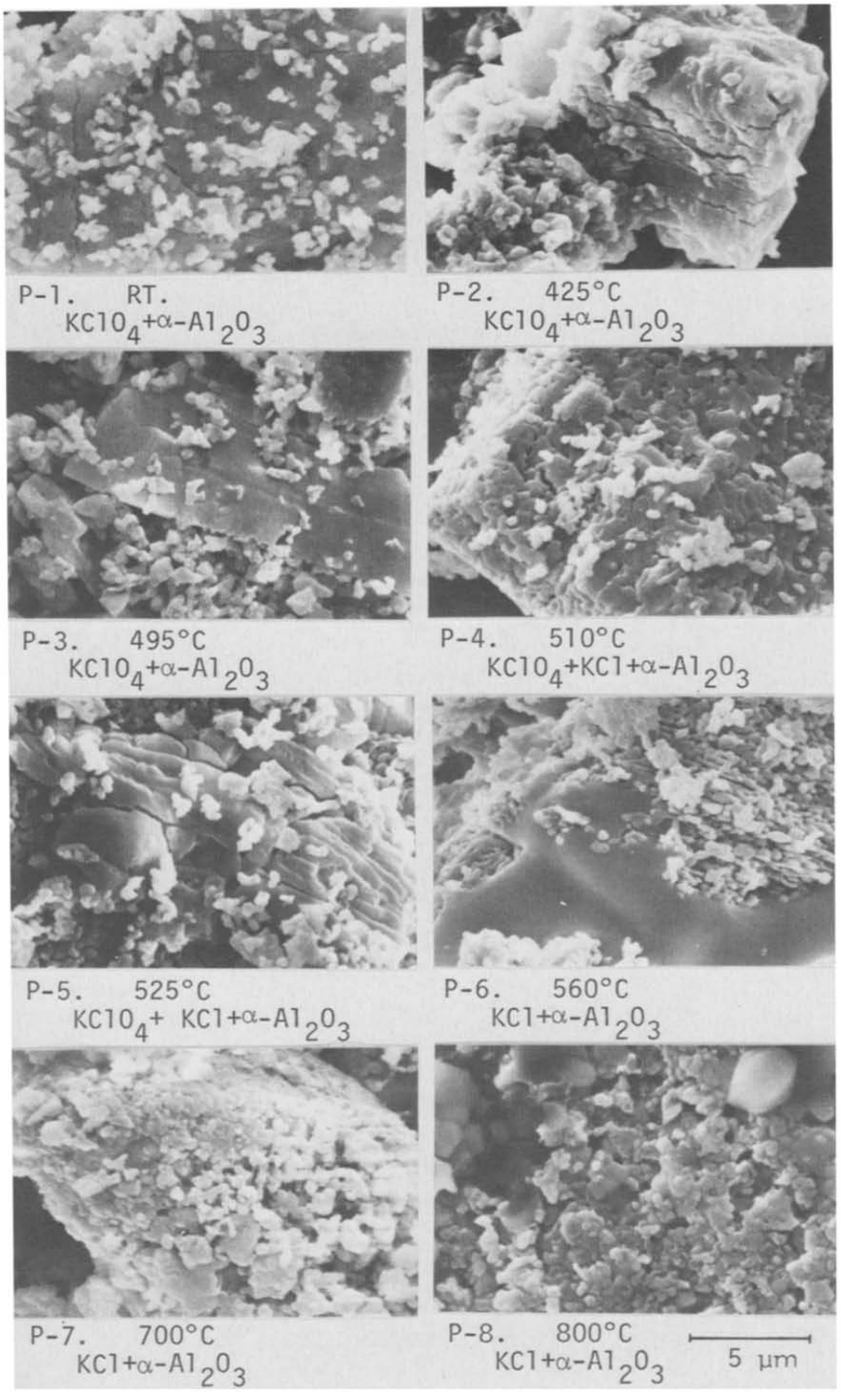

Fig. (2-B). SEM photographs showing the thermal decomposition of the $KClO_4$—α-Al_2O_3 mixture.

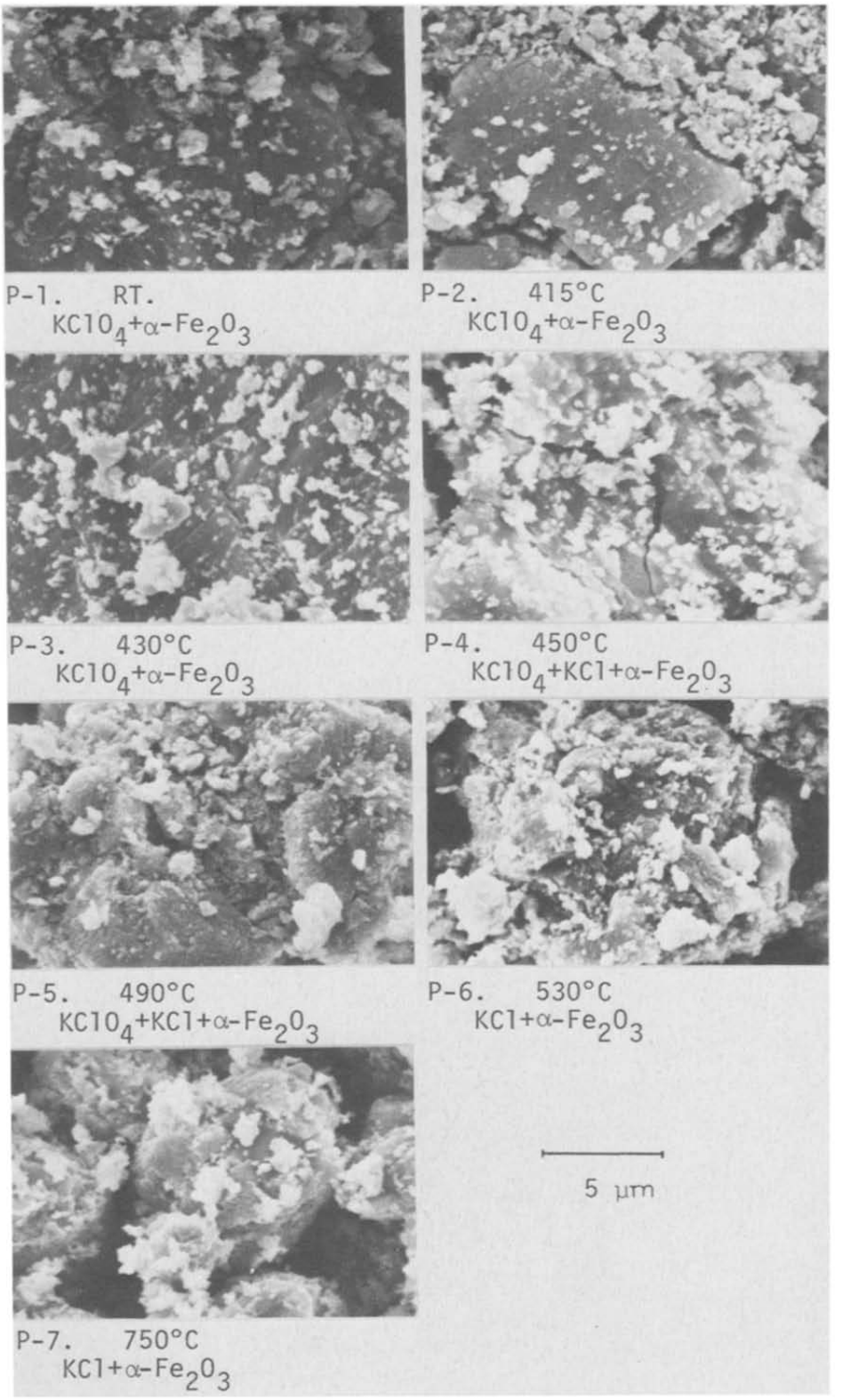

Fig. (2-C). SEM photographs showing the thermal decomposition of the $KClO_4$—α-Fe_2O_3 mixture.

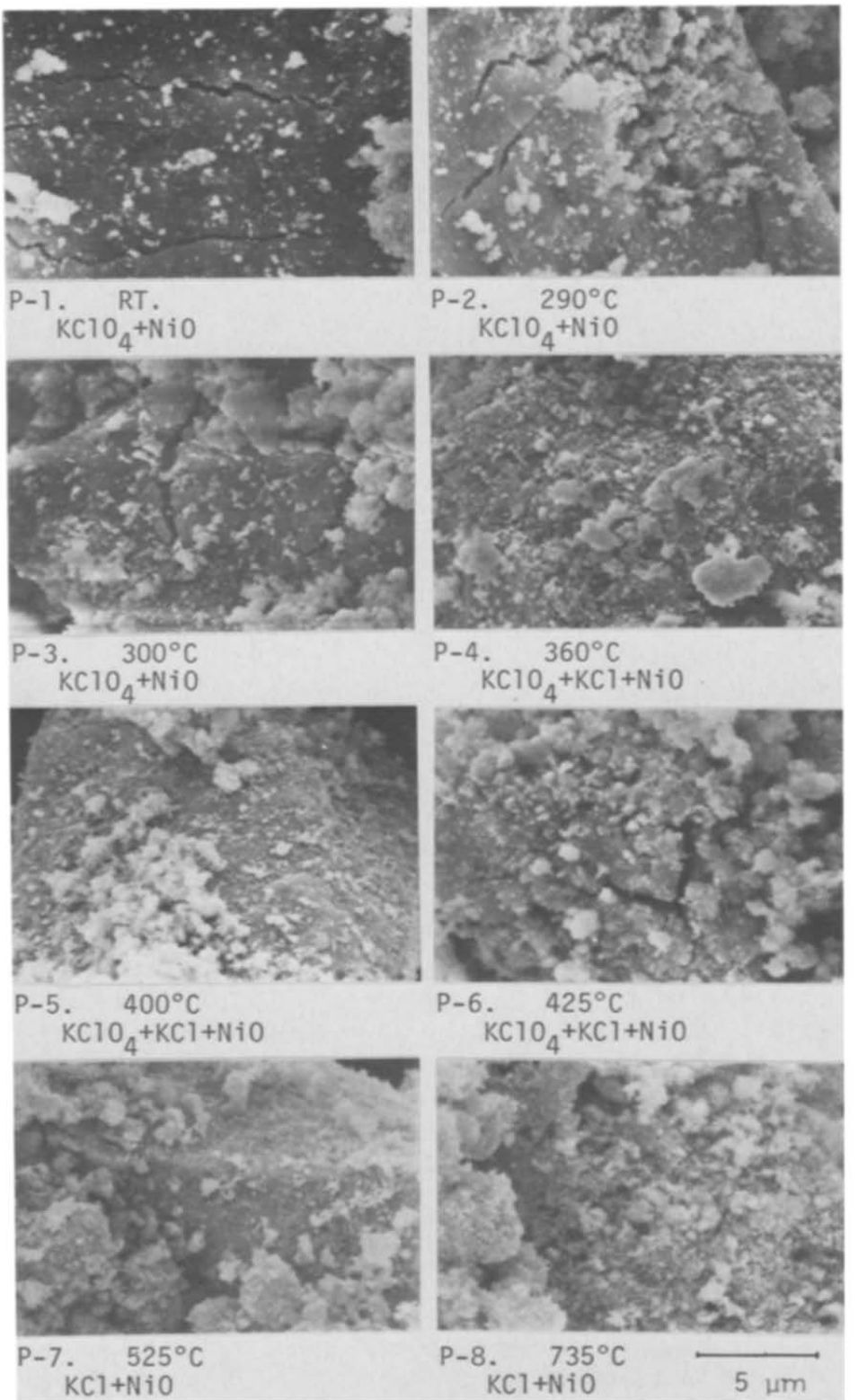

Fig. (2-D). SEM photographs showing the thermal decomposition of the $KClO_4$—NiO mixture.

perature give similar photographs to P-1. P-4 corresponds to the sample heated to 510°C where the endothermic peak due to the melting of $KClO_4$ starts as shown in Fig. 2, curve (2-B). In this sample, a small amount of KCl was observed by X-ray analysis. P-4 shows that small $KClO_4$ particles sinter to adhere. P-5 shows the sample obtained during melting of $KClO_4$ after heating to 525°C. It is seen that $KClO_4$ in the molten state is solidified and grows into large particles. After having been decomposed in the liquid state up to 560°C, KCl with a smooth surface adheres to small particles of α-Al_2O_3 as shown in P-6. P-7 and P-8 correspond to KCl—α-Al_2O_3 mixtures before (700°C) and after (800°C) the melting of KCl. After melting, the KCl grows into large particles.

(iii) $KClO_4$—α-Fe_2O_3 mixture

The DTA curve of this mixture is shown in Fig. 2, curve (2-C). The pattern of the DTA curve is different from that of pure $KClO_4$ and the $KClO_4$—α-Al_2O_3 mixture. After the crystallographic transformation (endotherm at 307°C), the broad exothermic peak starts at 450°C, which suggests an occurrence of solid state decomposition of $KClO_4$. KCl formed by the solid state decomposition yields the small sharp endothermic peak at 507°C by forming a eutectic mixture with undecomposed $KClO_4$, which is followed by the sharp exothermic peak at 510°C due to the decomposition of $KClO_4$ in the liquid state.

SEM photographs are shown in Fig. (2-C). P-1 is the mixture of $KClO_4$ and α-Fe_2O_3 at room temperature before reaction. As in the case of the $KClO_4$—α-Al_2O_3 mixture, small white α-Fe_2O_3 particles are scattered on the surface of large $KClO_4$ crystals. P-2 and P-3 show samples heated to 415 and 430°C, respectively, after the crystallographic transformation, which are similar to P-1. The exothermic peak of the solid state decomposition starts at 450°C at which partial decomposition is recognized by X-ray diffraction of the sample. The sample removed at 450°C gives P-4. No serious distinctions are observed between P-4 and P-3, except for the formation of small round swellings on the $KClO_4$ surface. P-4 does not show indications of melting. P-5 corresponds to the state at the top of the broad exothermic peak at 490°C in Fig. 2, curve (2-C). It is observed in P-5 that the agglomeration of small particles forms a large particle. At 530°C, after the decomposition, the sample (P-6) shows similar shape of particles to that observed before the decomposition, in contrast to pure $KClO_4$ and the $KClO_4$—α-Al_2O_3 system, Fig. (2-A), P-8 and Fig. (2-B), P-6. P-7 in Fig. (2-C) shows the KCl—α-Fe_2O_3 mixture at 750°C after melting of KCl.

(iv) $KClO_4$—NiO mixture

The DTA curve of this mixture is shown in Fig. 2, curve (2-D). The broad exothermic deflection is observed just after the endothermic crystallographic transformation at 310°C. X-Ray analysis revelaed that the sample heated up to 360°C contains KCl decomposition product. Accordingly, the broad exothermic peak is considered to be due to the decomposition.

In Fig. (2-D), P-1 is the mixture before the reaction. Nickel oxide is seen as small white particles on the surface of a large $KClO_4$ crystal with cracks. P-

2 and P-3, for samples heated to 290 and 300°C, resemble P-1. At 360°C, where the DTA curve starts to deflect toward the exothermic direction, X-ray analysis showed the formation of a small amount of KCl in the sample, which shows the porous surface of $KClO_4$ as seen in P-4; however, no indication of melting can be detected. P-5 and P-6 correspond to more advanced reaction stages than P-4, and P-7 and P-8 correspond to the stages after the decomposition. P-7 and P-8 are not different from P-4.

It was suggested from the DTA curves and SEM photographs described above that the liquid state decomposition proceeds after the melting of the perchlorate in the cases of pure $KClO_4$ and the $KClO_4$—α-Al_2O_3 mixture, in contrast to the solid state decomposition in the cases of the $KClO_4$—α-Fe_2O_3 and $KClO_4$—NiO mixtures. As seen in Fig. 2 curves (2-A) and (2-B), the endothermic DTA peak due to melting of $KClO_4$ is at 605°C for pure $KClO_4$ and at 535°C for the $KClO_4$—α-Al_2O_3 mixture. Do these temperatures mean that α-Al_2O_3 does not promote the solid state decomposition, but lowers the melting temperature? This was examined in following experiments.

Harvey et al. [8] have reported that the melting temperature of $KClO_4$ is lowered by mixing it with KCl. Figure 3 shows the DTA curves of $KClO_4$ containing KCl at various mixing ratios from 10 to 100% $KClO_4$. These curves reveal that the endothermic DTA melting peak starts at about 580°C in the case of 100% $KClO_4$ (curve 7) and at about 505°C in the cases of $KClO_4$—KCl mixtures (curves 1—6) irrespective of the change in mixing ratio. Figure 4 curves 1—6 show the DTA results obtained for samples of α-Al_2O_3 (0.5 g) mixed with $KClO_4$—KCl mixtures (0.5 g) of the various mixing ratios shown in Fig. 3. Curve 7 is the DTA curve for the $KClO_4$—α-Al_2O_3 mixture. $KClO_4$—KCl—α-Al_2O_3 mixtures give the starting temperature of DTA melting peak at 495°C irrespective of the mixing ratio of KCl to $KClO_4$. The $KClO_4$—α-Al_2O_3 mixtures gives 510°C. The results in Figs. 3 and 4 indicated that KCl leads to a lowering of the melting temperature of $KClO_4$, and that $KClO_4$—KCl, $KClO_4$—KCl—α-Al_2O_3, and $KClO_4$—α-Al_2O_3 mixtures give similar starting temperatures for melting, that is, 505, 495 and 510°C, respectively. It is considered that the lowering of the melting temperature is a result of the formation of KCl, and thus the lower melting temperature of the $KClO_4$—α-Al_2O_3 mixture is due to the formation of KCl from the solid state decomposition of $KClO_4$ by α-Al_2O_3, but the amount of KCl formed by the solid state decomposition is so small that X-ray analysis, SEM and DTA cannot detect it.

Potassium Chlorate

Figure 5 shows the DTA curves for the thermal decomposition of $KClO_3$, $KClO_3$—α-Al_2O_3, and $KClO_3$—α-Fe_2O_3 mixtures. SEM photographs are shown in Figs. (5-A)—(5-C).

(i) Pure $KClO_3$

According to previous studies [9—11] of pure $KClO_3$, the endothermic peak at 370°C and the two exothermic peaks at 540 and 580°C in Fig. 5, curve (5-A) correspond to the melting of $KClO_3$, the disproportionation of the chlorate to $KClO_4$ and the decomposition of the $KClO_4$ formed, respectively.

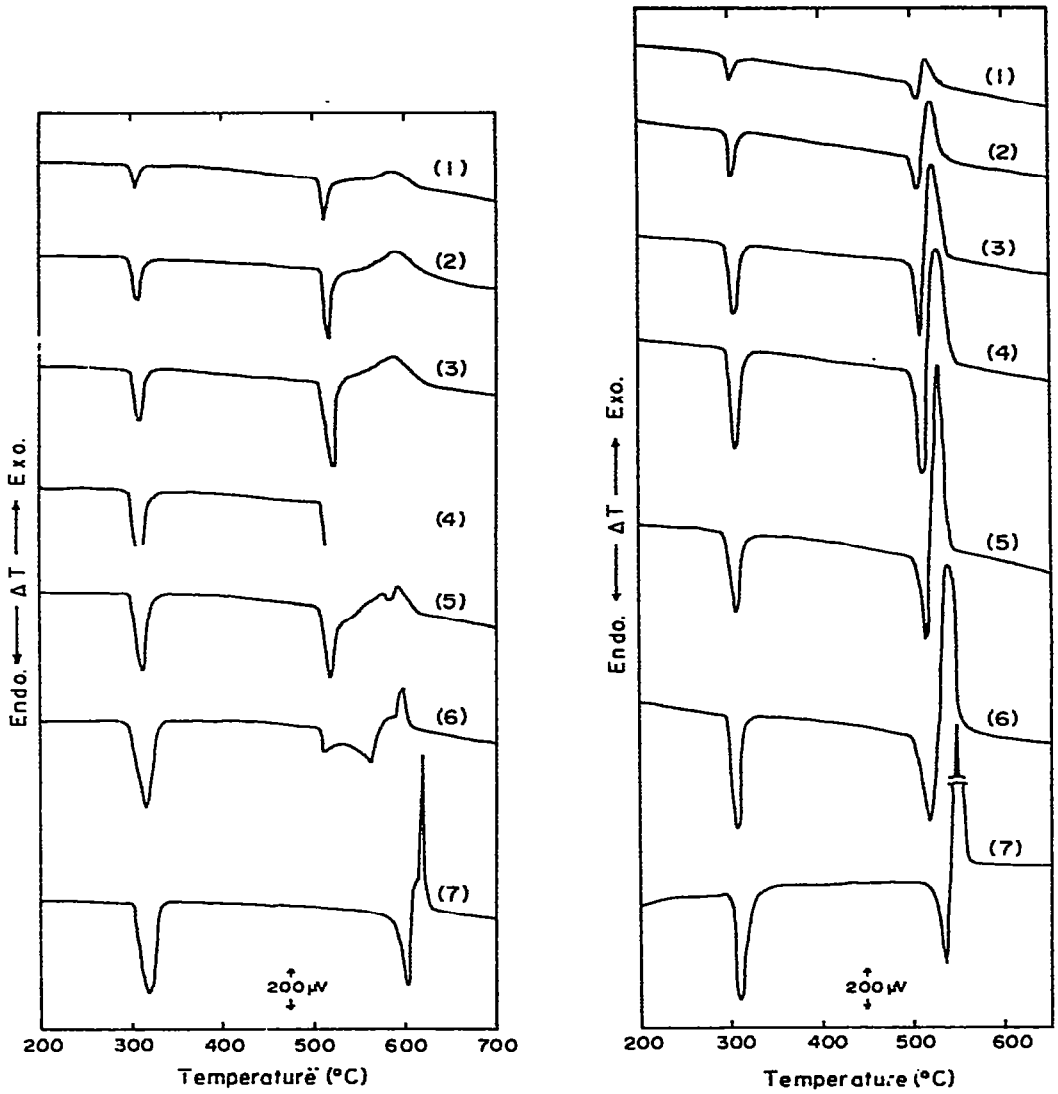

Fig. 3. DTA curves of $KClO_4$—KCl mixtures. (1) 10 mole % $KClO_4$ + 90 mole % KCl; (2) 20 mole % $KClO_4$ + 80 mole % KCl; (3) 40 mole % $KClO_4$ + 60 mole % KCl; (4) 60 mole % $KClO_4$ + 40 mole % KCl; (5) 80 mole % $KClO_4$ + 20 mole % KCl; (6) 90 mole % $KClO_4$ + 10 mole % KCl; (7) 100 mole % $KClO_4$. Heating rate, 4.6°C min^{-1}; atmosphere, static air.

Fig. 4. DTA curves of $KClO_4$ + KCl + α-Al_2O_3 mixtures. Heating rate, 4.6°C min^{-1}; atmosphere, static air. Sample consists of 0.5 g α-Al_2O_3 and 0.5 g $KClO_4$—KCl mixture. Mixing ratios of samples for curves (1)—(7) are same as those for Fig. 3, curves (1)—(7).

In Fig. (5-A), P-1 shows the $KClO_3$ sample before decomposition. P-2 and P-3 indicate that no change occurs after heating to 325°C (just before melting) and to 345°C (initial stage of melting). However, as found from P-4, after melting (390°C) the number of cracks increases compared with P-2 and P-3. This increase may arise from rapid cooling of the $KClO_3$ melt. X-Ray analysis revealed the formation of $KClO_4$ and the remaining $KClO_3$ in the

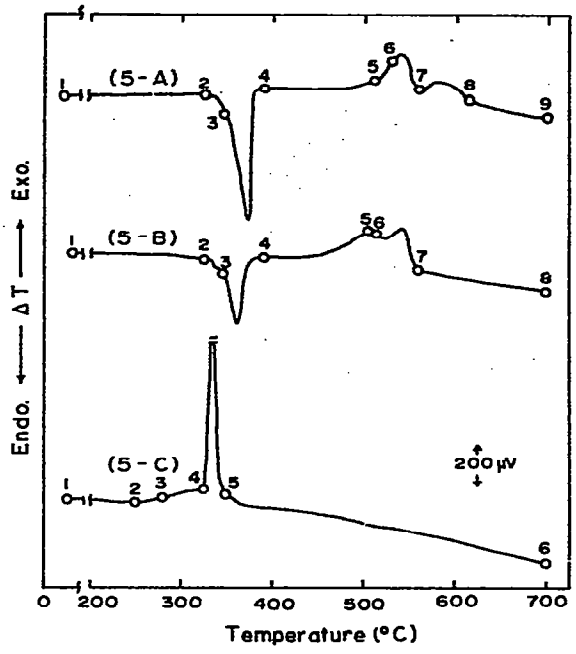

Fig. 5. DTA curves of $KClO_3$ systems. (5-A), $KClO_3$; (5-B), $KClO_3 + \alpha\text{-}Al_2O_3$; (5-C), $KClO_3 + \alpha\text{-}Fe_2O_3$. Heating rate, 4.6°C min^{-1}; atmosphere, static air; mixing ratio, 1 : 1 by weight. Circles indicate the temperatures at which the samples were removed and the numbers appended to the circles correspond to photograph numbers in Figs. (5-A)—(5-C).

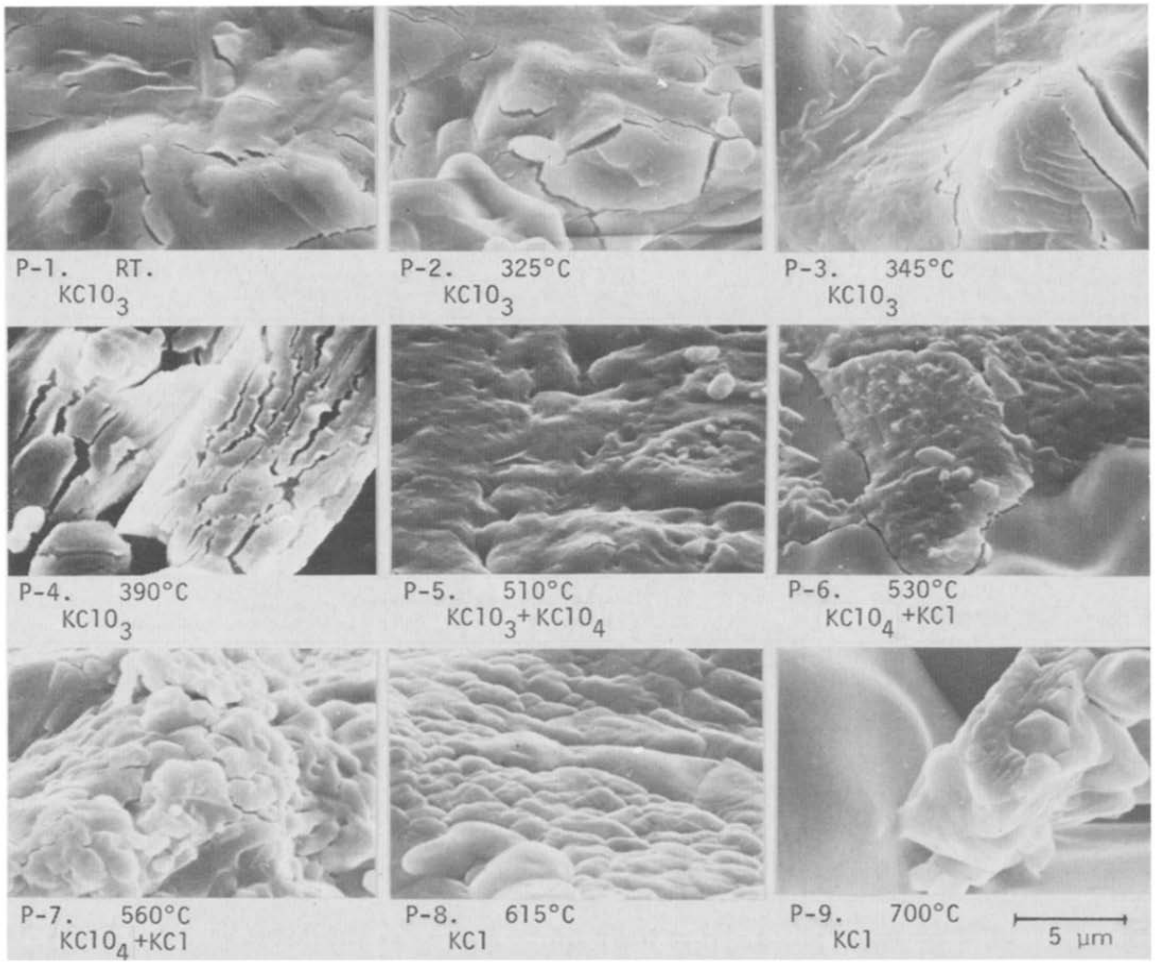

Fig. (5-A). SEM photographs showing the thermal decomposition of pure $KClO_3$. Heating temperature and X-ray result of the samples are indicated below each photograph.

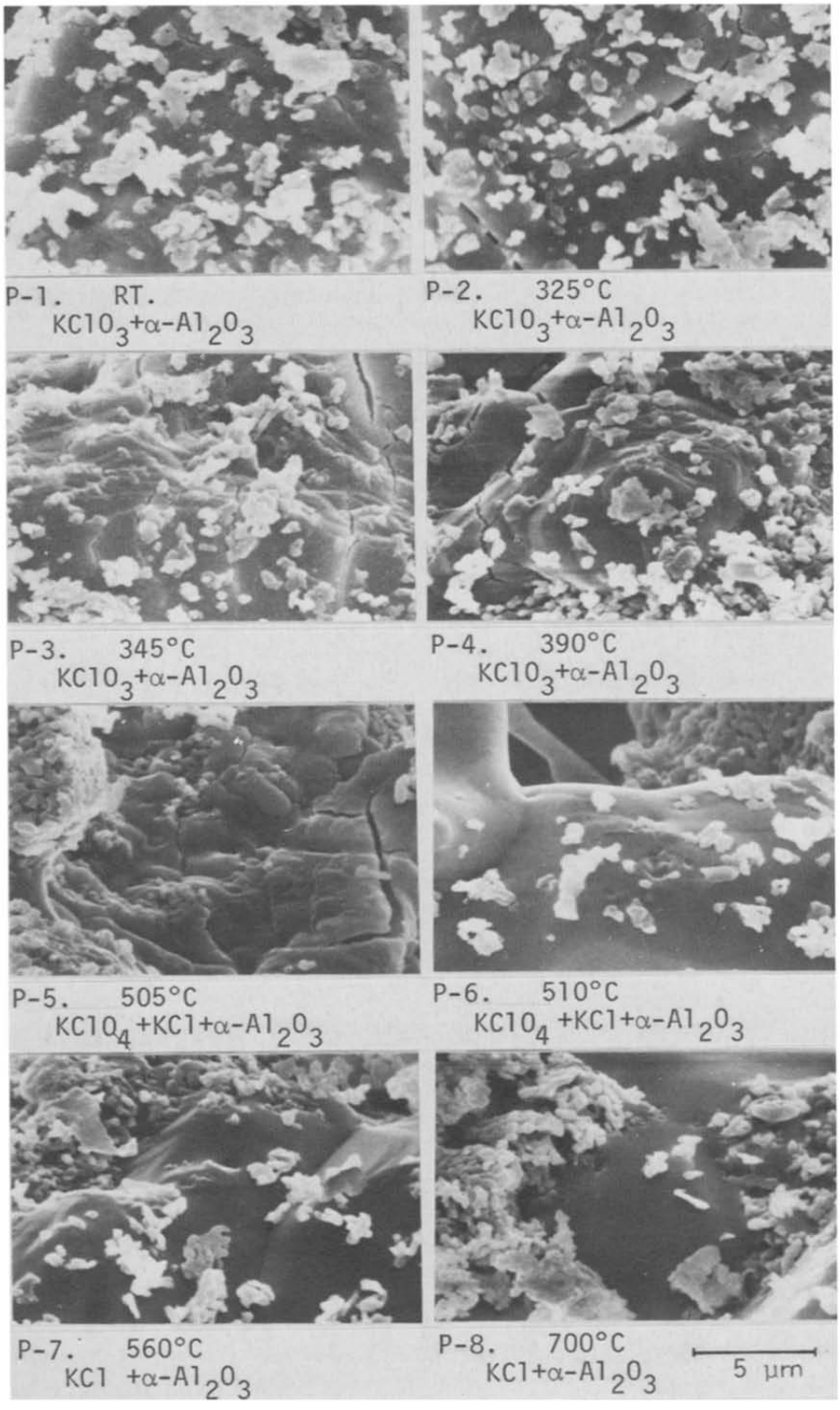

Fig. (5-B). SEM photographs showing the thermal decomposition of the $KClO_3$—α-Al_2O_3 mixture.

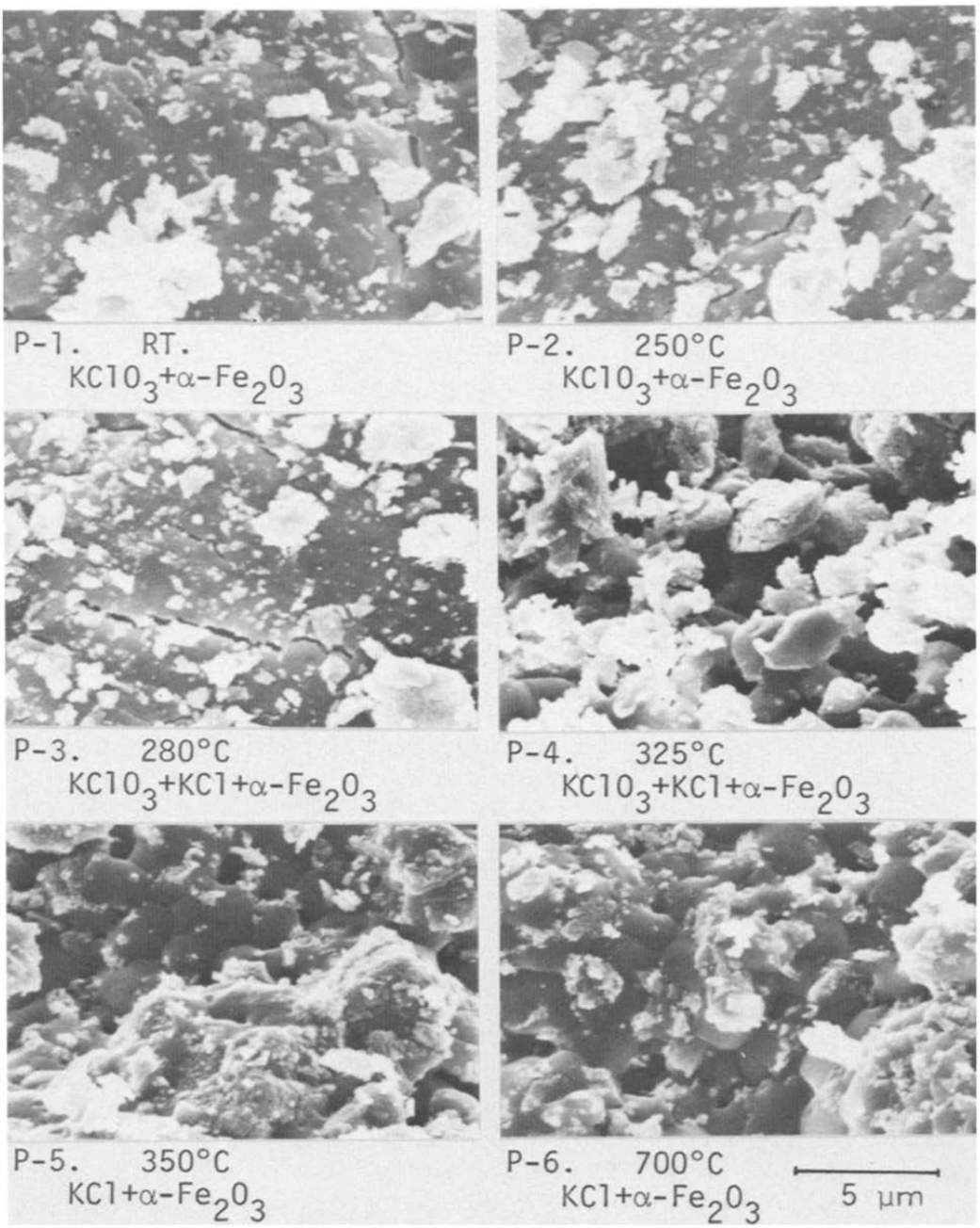

Fig. (5-C). SEM photographs showing the thermal decomposition of the $KClO_3$—α-Fe_2O_3 mixture.

sample heated up to 510°C (P-5) at the beginning stage of first exothermic peak shown in Fig. 5, curve (5-A). As seen in P-5, this sample gives a different SEM photograph from P-1—P-4 before the reaction. P-5 is similar to Fig. (2-A), P-7 which represents the surface of pure molten $KClO_4$. P-6 corresponds to the sample heated to 530°C in the neighborhood of the top of the first exothermic peak. The composition of the sample was $KClO_4$ + KCl. P-6 indi-

cates two parts, with smooth and rough surfaces. The rough surface resembles that of $KClO_3$ + $KClO_4$ shown in P-5, and thus the smooth part may be the surface of the KCl formed. At 560°C, where the first exothermic peak terminates, as shown in P-7 the sample composition is $KClO_4$ + KCl which is the same as that for P-6, but the smooth part seen in P-6 disappears to become clusters of small particles. After the decomposition, P-8 (615°C) and P-9 (700°C) are similar to KCl as shown in Fig. (2-A), P-9 and P-10.

(ii) $KClO_3$—α-Al_2O_3 mixture

Figure 5, curve (5-B) is the DTA curve of the $KClO_4$—α-Al_2O_3 mixture. The pattern of the curve is similar to that of pure $KClO_3$, Fig. 5, curve (5-A), but it can be seen that the DTA peaks for melting and decomposition are shifted to lower temperature ranges.

Figure (5-B), P-1 and P-2 correspond to samples removed at room temperature and at 328°C just before $KClO_3$ melting, respectively. Particles of α-Al_2O_3 are observed as small white particles scattered on the $KClO_3$ crystal. P-3 and P-4 show samples obtained at 345°C where the endothermic melting peak starts and at 390°C where it terminates. These photographs show that α-Al_2O_3 particles were embedded in the surface layer of $KClO_3$ as the result of melting of the chlorate. X-Ray analysis of samples removed at 505 and 510°C revealed that, at the top of exothermic disproportionation peak, $KClO_3$ changed completely into $KClO_4$ and the composition is $KClO_4$ + KCl + α-Al_2O_3. P-5 and P-6 correspond to these samples, which show the agglomeration of small particles and the solid mass of smooth surface resembling Fig. (2-B), P-5. After the decomposition as seen in P-7 (560°C) and P-8 (700°C), KCl forms masses of smooth surface. P-5—P-8 give an indication of the solidification of the molten phase.

(iii) $KClO_3$—α-Fe_2O_3 mixture

Figure 5, curve (5-C) is the DTA curve of the $KClO_3$—α-Fe_2O_3 mixture. It is found that the curve starts to deflect towards the exothermic direction at about 250°C and gives an explosive exothermic peak between 325 and 350°C. Figure (5-C) shows the SEM photographs and the results of X-ray analysis. X-Ray analysis indicated that the sample heated to 280°C (P-3) contains a small amount of KCl and that heated to 350°C (P-5) after the explosive DTA peak consists of KCl and α-Fe_2O_3. These results suggest that the exothermic peak appearing between 250 and 350°C results from the decomposition of $KClO_3$. In contrast to the cases of pure $KClO_3$ and the $KClO_3$—α-Al_2O_3 mixture, the formation of $KClO_4$ is not detected by X-ray analysis of samples of $KClO_3$—α-Fe_2O_3 mixture. Therefore, it is considered that the disproportionation reaction of $KClO_3$ to $KClO_4$ is absent and α-Fe_2O_3 preferentially promotes the decomposition of $KClO_3$ into KCl.

In Fig. (5-C), P-1 and P-2 show the sample before heating and that heated up to 250°C, respectively. The white particles of α-Fe_2O_3 are seen on the $KClO_3$ surface. P-3 corresponds to the sample heated up to 280°C. This does not show any distinguishable differences from P-1 and P-2, although the sample for P-3 contains a small amount of KCl. As observed in P-4, the porous aggregation of particles of 2—4 μm are found at 325°C just before the explo-

sive exothermic peak. Furthermore, the particles are seen to be classified into exothermic peak. Furthermore, te particles are seen to be classified into those of smooth and rough surface. P-5 and P-6 are KCl—α-Fe_2O_3 mixtures obtained after the decomposition, which show the sintering of particles accompanying the decrease in porosity and the disappearance of the particles of rough surface.

Potassium Bromate

Figure 6 shows the DTA curves of the $KBrO_3$ systems. Figures (6-A)—(6-C) are SEM photographs and X-ray results of samples obtained by heating the systems to the temperatures shown by circles on the DTA curves.

(i) Pure $KBrO_3$

Figure 6, curve (6-A) is the DTA curve of pure $KBrO_3$. Two sharp peaks at 425°C (endothermic) and at 430°C (exothermic) correspond to melting and the decomposition of the $KBrO_3$ melt, respectively [3,12,13].

In Fig. (6-A), P-1 is an SEM photograph of pure $KBrO_3$ before the reaction. P-2 corresponds to the sample at 380°C, just before melting of the bromate, which is similar to P-1. P-3 shows the sample heated to 410°C during melting. This sample was found to contain a very small amount of product KBr by X-ray analysis. P-3 indicates an interesting change in the surface of the sample, that is, the formation of a region consisting of circular and elliptical swellings. This region is thought to be due to sintering between two large

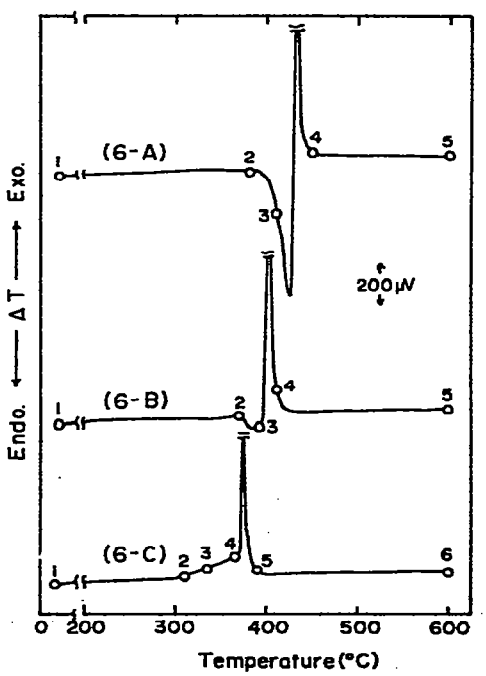

Fig. 6. DTA curves of $KBrO_3$ systems. (6-A), $KBrO_3$; (6-B), $KBrO_3$ + α-Al_2O_3; (6-C), $KBrO_3$ + α-Fe_2O_3. Heating rate, 4.6°C min^{-1}; atmosphere, static air; mixing ratio, 1 : 1 by weight. Circles indicate the temperatures at which the samples were removed and the numbers appended to the circles correspond to photograph numbers in Figs. (6-A)—(6-C).

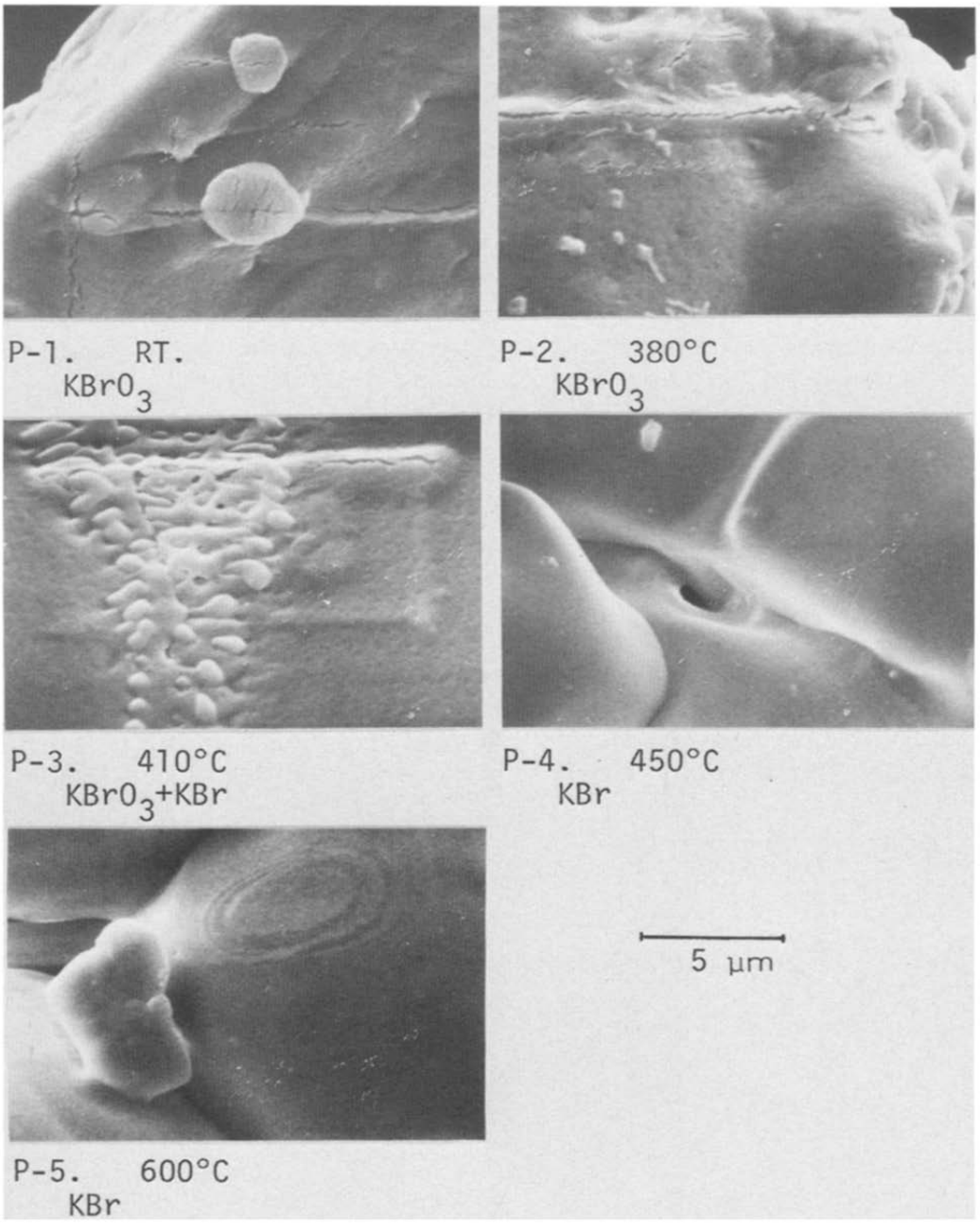

Fig. (6-A). SEM photographs showing the thermal decomposition of pure $KBrO_3$. Heating temperature and X-ray result of the samples are indicated below each photograph.

particles of partly molten $KBrO_3$. P-4 and P-5 correspond to KBr particles formed after the decomposition, which show smooth surfaces.

(ii) $KBrO_3$—α-Al_2O_3 mixture

The DTA curve of the $KBrO_3$—α-Al_2O_3 mixture is shown in Fig. 5, curve (6-B). The pattern of the curve is similar to that of pure $KBrO_3$, but the peak

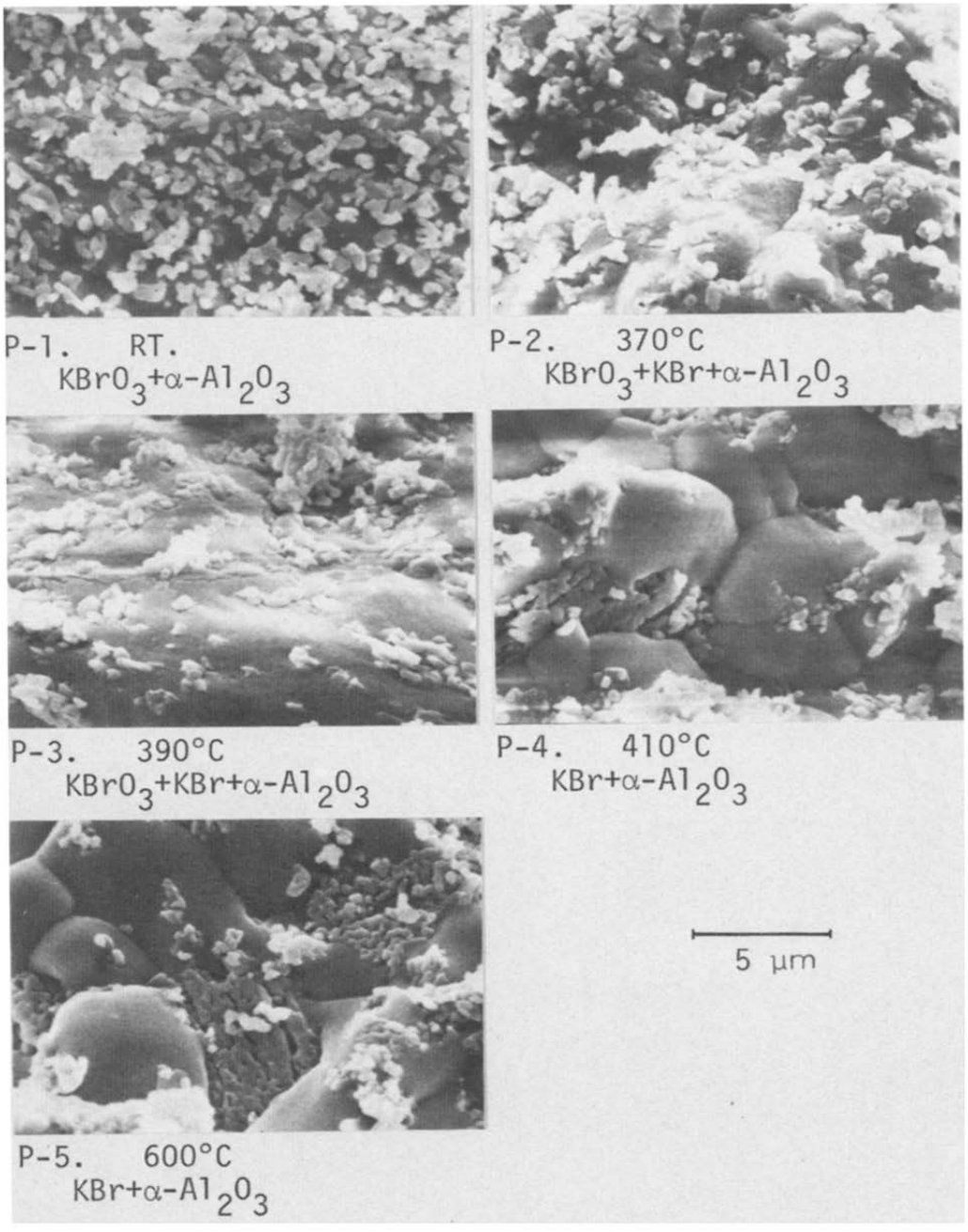

Fig. (6-B). SEM photographs showing the thermal decomposition of the $KBrO_3$—α-Al_2O_3 mixture.

area of melting becomes smaller and the peak temperatures are lower than the cases of pure $KBrO_3$.

Figure (6-B), P-1 shows the sample at room temperature, in which the small α-Al_2O_3 particles are observed on the $KBrO_3$ surface. P-2 corresponds to the sample heated to 370°C at the initial stage of the endothermic DTA peak. X-Ray analysis of this sample indicated the formation of a very small

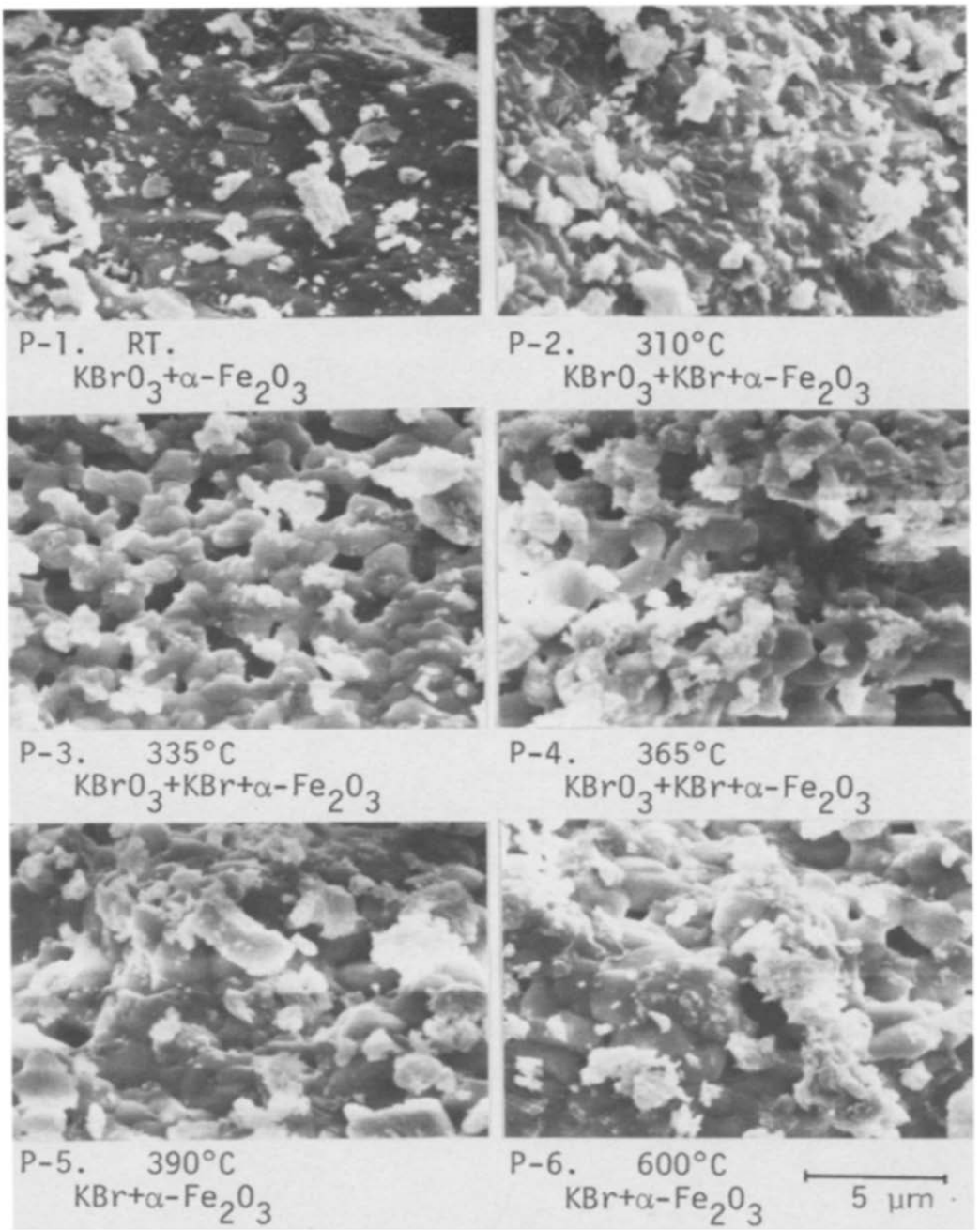

Fig. (6-C). SEM photographs showing the thermal decomposition of the $KBrO_3$—α-Fe_2O_3 mixture.

amount of KBr. No marked difference is observed between P-1 and P-2, except, to some extent, the surface roughening. P-3 shows the sample heated to 390°C at the bottom of the endothermic peak, which consists of $KBrO_3$, KBr and α-Al_2O_3. It is observed in P-3 that α-Al_2O_3 particles are embedded in the surface layer of molten $KBrO_3$(+KBr). P-4 and P-5 show KBr with smooth surface and α-Al_2O_3 particle agglomentation after the decomposition.

(iii) $KBrO_3$—α-Fe_2O_3 mixture

Figure 6, curve (6-C) is the DTA curve of the $KBrO_3$—α-Fe_2O_3 mixture. The curve begins to give the gradual exothermic deflection near 300°C followed by the explosive exothermic peak at 375°C. There is no endothermic peak on the curve.

Figure (6-C), P-1 is the view before the reaction, which shows the relatively smooth surface of $KBrO_3$ and small white particles on it. At 310°C, just after the start of the broad exotherm, X-ray analysis of the sample revealed the decomposition of a very small amount of $KBrO_3$ and the SEM photograph shows the formation of many protrusions of about 1 μm as seen in P-2. With the progress of the decomposition, the sample removed at 335°C (P-3) shows the connection of particles of 2—4 μm and the formation of pores of similar size. P-3 gives no indication of embedded additive particles, in contrast with the case of $KBrO_3$—α-Al_2O_3, Fig. (6-B), P-3. Therefore, it is considered that α-Fe_2O_3 promotes the solid state decomposition of $KBrO_3$. P-4 corresponds to the sample heated to 365°C just before the explosive exothermic peak, which shows the growth of particles compared with those seen in P-3. P-5 and P-6 are SEM photographs of the KBr—α-Fe_2O_3 mixture formed after the decomposition, which show extensively different views from the KBr—α-Al_2O_3 mixture, Fig. (6-B), P-4 and P-5.

Potassium Periodate

Figure 7, curves (7-A)—(7-C) are the DTA curves of the KIO_4 systems. The SEM and X-ray results are shown in Figs. (7-A)—(7-C).

(i) Pure KIO_4

Figure 7, curve (7-A) is the DTA curve of pure KIO_4. As shown in previous papers [3,14], the sharp exothermic peak at 320°C corresponds to the decomposition of KIO_4 into KIO_3 and the peak temperature was not affected by the additive. Two endothermic peaks appearing near 540 and 570°C are due to the melting and decomposition of KIO_3 formed.

Figure (7-A), P-1 shows pure KIO_4 before the reaction. P-2, P-3 and P-4 correspond to samples removed at 285, 300 and 310°C, before the sharp decomposition exotherm of KIO_4 to KIO_3. These photographs show the formation of white spots on the KIO_4 surface and their growth with increasing temperature. X-Ray analysis of the sample showed that, at 320°C, KIO_4 was completely transformed into KIO_3. P-5 shows this sample forming an agglomeration of small KIO_3 particles. Any indications of melting of the sample are not observed in P-5. After heating to 500°C, the sample remains unchanged as KIO_3, but, as seen in P-6 and P-7, KIO_3 particles increase in size. P-8 shows the sample heated to 520°C in progress of the endothermic peak at 540°C. The change in composition was not detected by X-ray analysis of the sample; however, the very closely packed large KIO_3 particles with smooth surface are observed in P-8. P-9 is the SEM view of the sample heated to 555°C after the endothermic peak at 540°C and its composition was KIO_3 + KI. From these facts, it may be found that the endothermic peak at 540°C arises from the melting of KIO_3 and its decomposition in the liquid

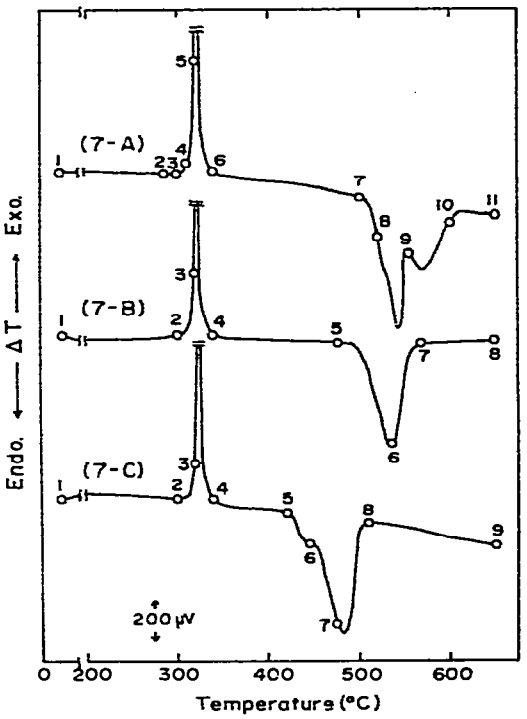

Fig. 7. DTA curves of KIO_4 systems. (7-A), KIO_4; (7-B), KIO_4 + α-Al_2O_3; (7-C), KIO_4 + + α-Fe_2O_3. Heating rate, 4.6°C min^{-1}; atmosphere, static air; mixing ratio, 1 : 1 by weight. Circles indicate the temperatures at which the samples were removed and the numbers appended to the circles correspond to the photograph numbers in Figs. (7-A)—(7-C).

phase. P-9 shows a decrease in the size of particles observed in P-8 and formation of pores. P-10 and P-11 were obtained for samples heated to 610 and 650° C, which show the large KI particles formed from molten KIO_3.

(ii) KIO_4—α-Al_2O_3 mixture

Figure 7, curve (7-B) is the DTA curve of the KIO_4—α-Al_2O_3 mixture. It is found that the addition of α-Al_2O_3 has no effect on the sharp exothermic peak for the decomposition of KIO_4 into KIO_3 around 320° C. The endothermic peak due to the decomposition of KIO_3 appears at 490—570° C and its shape is singlet.

Figure (7-B), P-1 shows the sample before the reaction. As seen from P-2, there is no change on heating to 300° C before the exothermic decomposition into KIO_3, in contrast to the case of the pure KIO_4 sample [Fig. (7-A), P-2 and P-3], where white spots were formed on the KIO_4 crystal. X-Ray analysis showed that the composition of samples heated to 320 and 340° C is KIO_3 + KIO_4 + α-Al_2O_3 and KIO_3 + α-Al_2O_3, respectively. As observed in P-3 and P-4, these samples are in a state of particle aggregation of 1—2 μm. At 475° C (P-5), the sample still remains as KIO_3, but the particles of 1—2 μm seen in P-4, increase in size to 4—5 μm, which is similar to P-6 in Fig. (7-A) for the pure KIO_4 sample. For the sample removed at the peak temperature of the endotherm (535° C), a considerable amount of KI was detected by X-

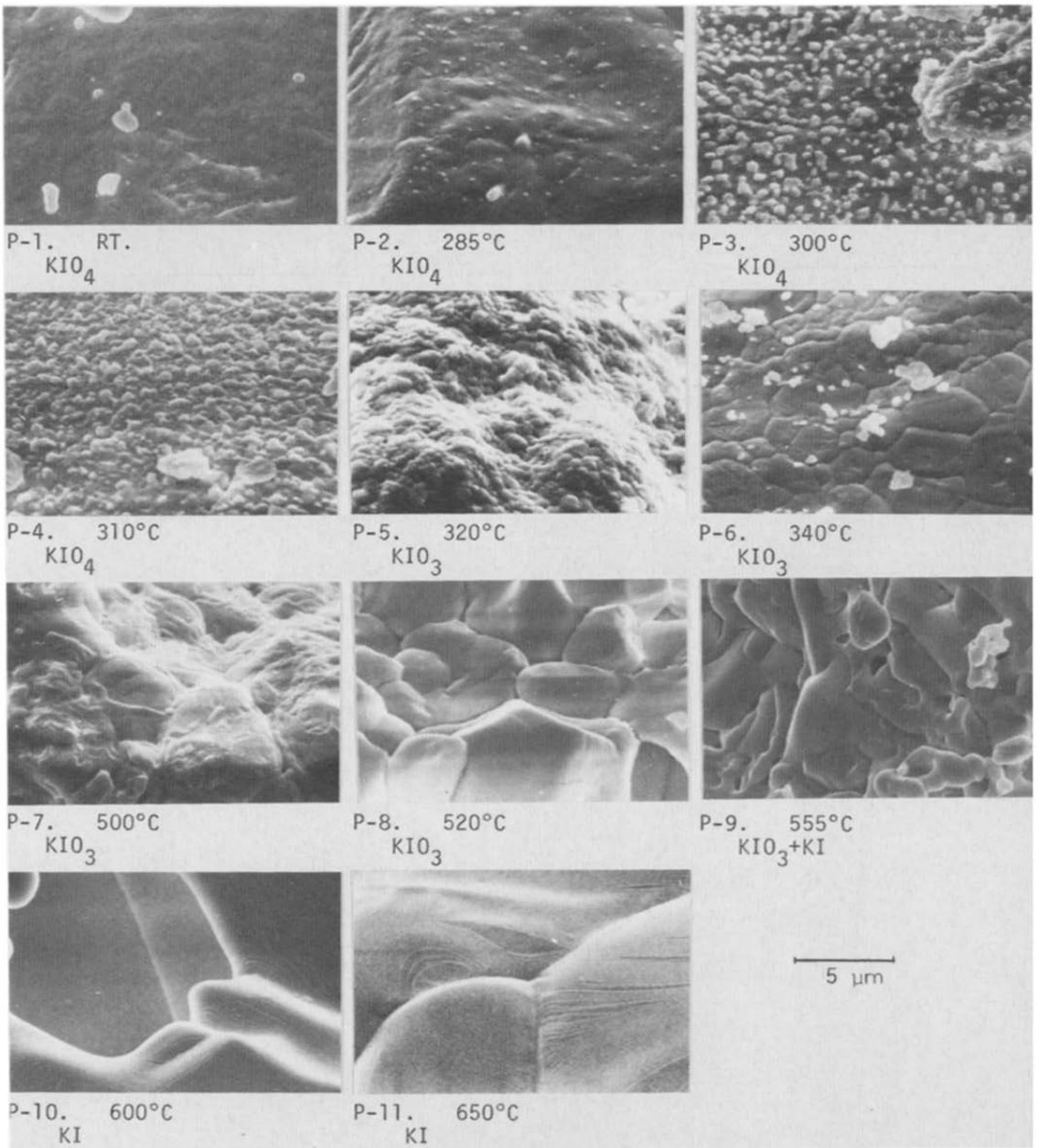

Fig. (7-A). SEM photographs showing the thermal decomposition of pure KIO_4. Heating temperature and X-ray result of the samples are indicated below each photograph.

ray analysis. As seen in P-6, this sample gives an indication of melting. P-7 and P-8 are photographs of the KI obtained after the decomposition of KIO_3.

(iii) KIO_4—α-Fe_2O_3 mixture

Figure 7, curve (7-C) shows the DTA curve of the KIO_4—α-Fe_2O_3 mixture. Addition of α-Fe_2O_3, as with α-Al_2O_3, does not affect the sharp exothermic peak at 325° C. The endothermic KIO_3 decomposition peak appears in a tem-

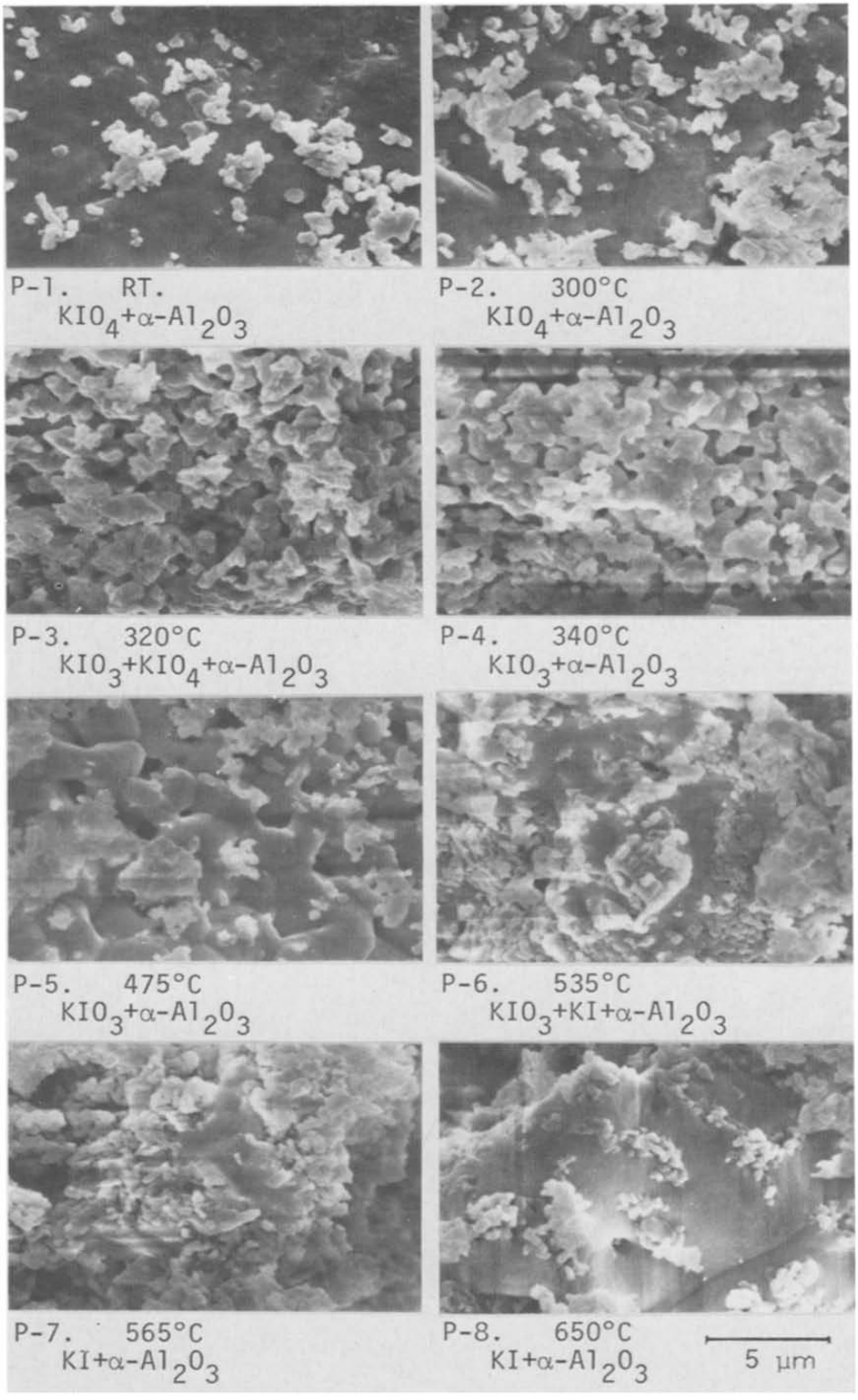

Fig. (7-B). SEM photographs showing the thermal decomposition of the KIO_4 + α-Al_2O_3 mixture.

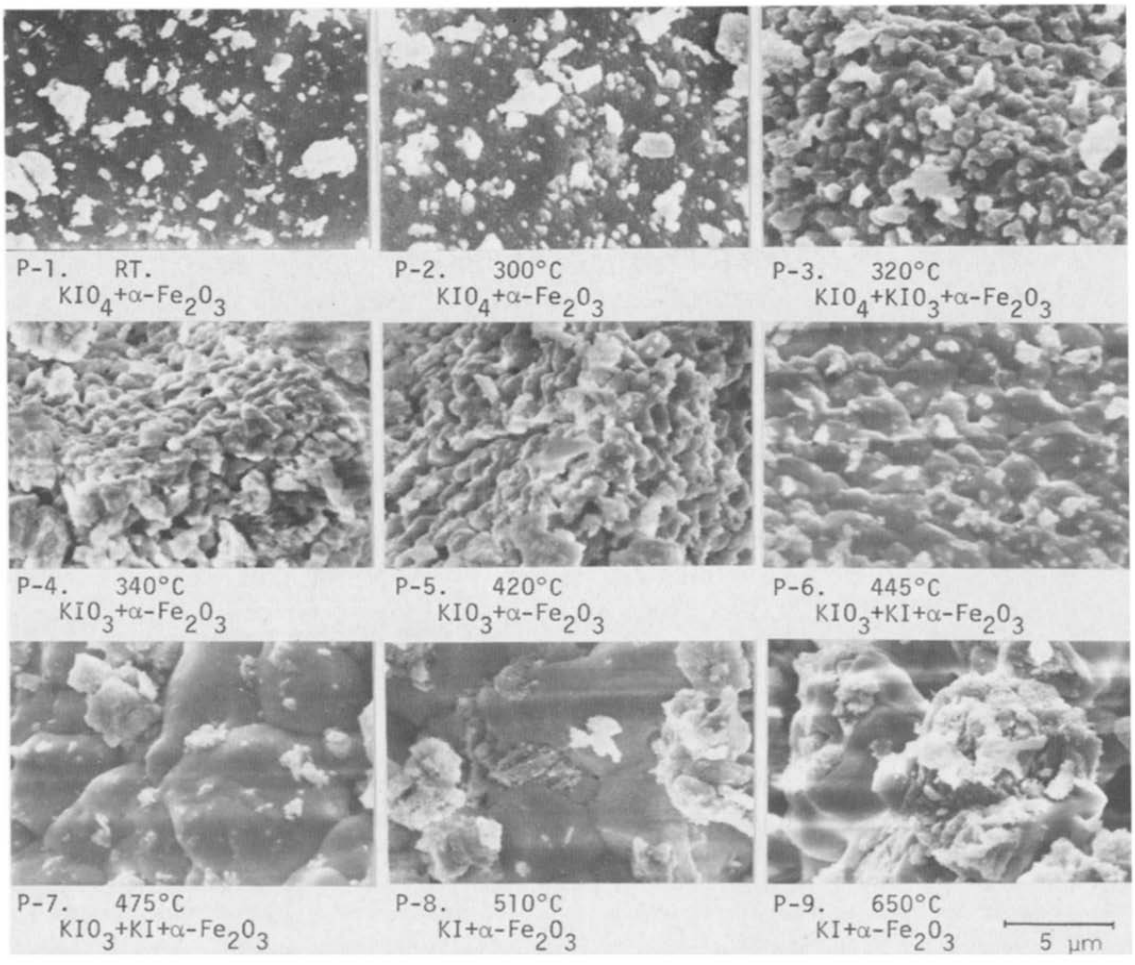

Fig. (7-C). SEM photographs showing the thermal decomposition of the KIO_4 + α-Fe_2O_3 mixture.

perature range of 420—510°C, which is lower by 70—80°C than the decomposition temperature of pure KIO_4 and the KIO_4—α-Al_2O_3 mixture.

In Fig. (7-C), P-1 corresponds to the sample before the reaction. P-2 is the photograph of the sample heated to 300°C, which is similar to P-1. P-3 corresponds to the sample in the course of decomposition into KIO_3 at 320°C. This photograph indicates the formation of many particles of 1 μm. The increase in heating temperature up to 420°C results in complete decomposition of KIO_4 into KIO_3. P-4 and P-5 show these samples having composition of KIO_3 + α-Fe_2O_3. These two photographs are very similar to Fig. (7-B), P-4 of the KIO_4—α-Al_2O_3 system. It is seen from Figs. (7-A)—(7-C) that the particle size of the KIO_3 formed in the KIO_4—α-Fe_2O_3 and KIO_4—α-Al_2O_3 systems is smaller than that formed in the pure KIO_4 system. Figure (7-C), P-6 shows the sample heated to 445°C, which contained a small amount of KI. The growth of particles to 2—4 μm is observed. The amount of KI was found by X-ray analysis to be greater than that of KIO_3 at 475°C. P-7, taken at 475°C, shows the formation of very large particles (5—8 μm) and into which

white α-Fe_2O_3 particles are embedded. Therefore, it is considered that the melting and the decomposition of sample proceed rapidly between 445 and 475°C. P-8 and P-9 show the KI + α-Fe_2O_3 mixture formed by the decomposition.

Potassium Iodate

The DTA experiments and SEM observations for KIO_3 systems were carried out in a similar way to the salts mentioned above. The results were the same as those obtained for the decomposition of KIO_3 formed in the KIO_4 systems.

CONCLUSIONS

In the present study, the apparatus does not permit SEM observations of a single sample heated in situ up to various temperatures in the course of the decomposition reaction, and powder samples were used. Therefore, the discussion was qualitative and contained many speculations. The authors, however, believe that the SEM observations confirmed the solid state decomposition by addition of α-Fe_2O_3.

REFERENCES

1 R. Furuichi, T. Ishii and K. Kobayashi, J. Therm. Anal., 6. (1974) 305.
2 M. Shimokawabe, R. Furuichi and T. Ishii, Thermochim. Acta, 20 (1977) 347; 21 (1977) 273; 24 (1978) 69.
3 R. Furuichi, T. Ishii, Z. Yamanaka and M. Shimokawabe, Thermochim. Acta, 51 (1981) 245.
4 W.K. Rudloff and E.S. Freeman, J. Phys. Chem., 74 (1970) 3317.
5 P.J. Herley, P.W.M. Jacobs and P.W. Levy, Proc. R. Soc. London, Ser. A, 318 (1970) 197.
6 K.J. Kraeutle, J. Phys. Chem., 74 (1970) 1350.
7 T. Ishii, R. Furuichi and Y. Kobayashi, Thermochim. Acta, 2 (1974) 39.
8 A.E. Harvey, M.T. Edmison, E.D. Jones, R.A. Seybert and K.A. Catto, J.Am. Chem. Soc., 76 (1954) 3270.
9 T. Ishii, K. Kamada and R. Furuichi, Kogyo Kagaku Zasshi, 74 (1971) 854.
10 W.K. Rudloff and E.S. Freeman, J. Phys. Chem., 73 (1969) 1209.
11 M.M. Markowitz, D.A. Boryta and H. Stwart, J. Phys. Chem., 68 (1964) 2282.
12 J. Jach, Proc. 4th Intern. Symp. on Reactivity of Solids, 1960, 63, 75.
13 J. Joseph and T.D. Randhakrishnan Nair, J. Therm. Anal., 14 (1978) 271.
14 B.R. Phillips and D. Taylor, J. Chem. Soc., (1963) 5583.